Heliyon

Received:
12 July 2018
Revised:
16 October 2018
Accepted:
13 March 2019

Cite as: Naveeda Firdous, Naveed Kausar Janjua. $CoPt_x/\gamma$-Al_2O_3 bimetallic nanoalloys as promising catalysts for hydrazine electrooxidation. Heliyon 5 (2019) e01380. doi: 10.1016/j.heliyon.2019.e01380

$CoPt_x/\gamma$-Al_2O_3 bimetallic nanoalloys as promising catalysts for hydrazine electrooxidation

Naveeda Firdous, Naveed Kausar Janjua*

Department of Chemistry, Quaid-i-Azam University, Islamabad 45320, Pakistan

* Corresponding author.

E-mail addresses: nkausarjanjua@yahoo.com, nkjanjua@qau.edu.pk (N.K. Janjua).

Abstract

Stable bimetallic catalysts composed of $CoPt_x/\gamma$-Al_2O_3 (x = Pt/Co molar ratio) were synthesized by wet impregnation method followed by calcination and the H_2 reduction. The powders were characterized using XRD, AAS, BET, SEM, EDX, TPR, and TPO techniques. The prepared catalysts were drop casted on the glassy carbon electrode (GCE) and catalytic performance was examined for hydrazine electrooxidation in alkaline medium *via* cyclic voltammetry (CV). All the compositions in $CoPt_x/\gamma$-Al_2O_3 series showed high responses towards hydrazine electrooxidation, however; high activity of $CoPt_{0.034}/\gamma$-Al_2O_3 catalyst inferred it as a best material with an anodic peak current (i_P) response of 200 μA at 0.86 V. The prominent electrochemical (EC) responses for this composition are attributed to better accessible surface area resulting in a fast electron transfer. The $CoPt_x/\gamma$-Al_2O_3 catalysts are reported as the robust and superior prospective materials for extensive electroanalytical and catalytic studies.

Keywords: Electrochemistry, Inorganic chemistry, Analytical chemistry, Materials chemistry, Physical chemistry

https://doi.org/10.1016/j.heliyon.2019.e01380
2405-8440/© 2019 Published by Elsevier Ltd. This is an open access article under the CC BY-NC-ND license (http://creativecommons.org/licenses/by-nc-nd/4.0/).

1. Introduction

Hydrazine (N_2H_4) fuel cell technology is highly advantageous for electronic devices and fuel cell applications with the advantages of CO-free products [1]. Hydrazine is a strong reducing agent and highly reactive base. Its major applications include rocket propellant, explosive in pyrotechniques, hydrogen source in fuel cells, halogen removal from waste water, oxygen scavenger from boilers, insecticides in agriculture, precursor to many pharmaceuticals, development of photographic compounds, textile dyes making, and blowing agents for plastics [2, 3, 4, 5]. In recent years, the catalytic decomposition of hydrazine is extensively used for hydrogen generation for fuel cell applications and other devices [6, 7, 8, 9, 10, 11, 12, 13]. Although, hydrazine has been reported in history as a therapeutic agent for the cure of tuberculosis, sickle cell anemia, and chronic diseases [14]. However, hydrazine is declared as a carcinogenic compound which can cause gene mutation and hepatotoxicity [15]. Environmental protection agency (EPA) has stated hydrazine and its derivatives as environmental pollutants and threshold value of hydrazine in effluents is set to 0.0001% [16].

By considering the significance of hydrazine, its precise and economical determination is still a challenging role to the chemists. Various methods have been reported for hydrazine detection such as, spectrophotometric [17], liquid chromatography [18], titrimetry [19], coulometry [20], amperometry [21], potentiometry [22], and voltammetry [23]. However, linear ranges of data with less precision results in the complexity of most methods [24]. On the other hand, the electrochemical studies offer various methodologies with quick response time, greater sensitivity, simple operation, ease of miniaturization, and cost-effectiveness [25]. The mechanism and kinetics of hydrazine oxidation has been studied under a wide range of solution conditions and at different electrodes like silver [26], nickel [27], platinum [28], and carbon [29]. The mechanism of hydrazine electrooxidation mainly involves four-electron transfer with releases of N_2 gas as a final product as described in Eqs. (1) and (2) [30, 31]. The rate determining step involves one-electron transfer followed by a three-electron transfer to give N_2 as a final product.

$$N_2H_4 + H_2O \rightarrow N_2H_3 + H_3O^+ + e^- \text{ (slow)} \quad (1)$$

$$N_2H_3 + 3H_2O \rightarrow N_2 + 3H_3O^+ + 3e^- \text{ (fast)} \quad (2)$$

However, the electrooxidation of hydrazine at the surface of glassy carbon electrode is found kinetically slow due to large overpotential which is dependent on the nature of electrode material [32].

Accordingly, there is need to modify the electrode surface for fast electron transfer kinetics and to improve the detection limit [33]. This way, the desirable properties of

https://doi.org/10.1016/j.heliyon.2019.e01380
2405-8440/© 2019 Published by Elsevier Ltd. This is an open access article under the CC BY-NC-ND license (http://creativecommons.org/licenses/by-nc-nd/4.0/).

active material can be assigned directly to the electrode surface [34]. In this context, the design and development of novel electrocatalysts for hydrazine oxidation and detection has been focused [35,36, 37, 38]. Different types of modified electrodes including electrochemically pretreated glassy carbon electrode [39], carbon paste containing cobalt phthalocyanine [40], ultrafine platinum and ruthenium particles dispersed on porous carbon films [41, 42], poly (4-vinyl) pyridine-palladium film [43], ethylenediamine cellulose immobilized palladium NPs modified GCE [44], and cobalt hexacyanoferrate modified GCE [45] have depicted remarkable catalytic properties towards the electrooxidation of hydrazine. The modification of electrode surfaces had played a great role towards electron transfer kinetics and electrocatalytic studies [33]. The modified electrodes have a wide range of potential applications in the field of electrochemical technology, energy conversion, chemical analysis, electrochromic devices, and displays [34]. Metal nanoparticles (NPs) based electrocatalytic systems have advantages of high surface area, good durability, high dispersion, controlled particle size, morphology, chemical inertness, and good electrical/mechanical properties [46, 47, 48, 49, 50]. Bimetallic nanoparticle modified electrodes have been proved to be one of the most efficient electrode systems, owing to alloying effect between metal nanoparticles, and modification of electronic as well as chemical properties [51]. Bimetallic NPs modified electrodes display more advantages than monometallic counterparts, such as higher catalytic activity, better sensitivity, and longer life of electrode [52, 53].

Wan *et al.* prepared graphene nanoplatelets (GNPs) supported bimetallic Au-Pd nanoparticles and used as electrocatalysts for hydrazine oxidation. In comparison to monometallic catalysts, the oxidation peak potential and peak current values greatly improved for bimetallic nanoparticles [54]. In another study, bimetallic Au(Ni)/TiO_2-NTs catalysts were fabricated for the electrooxidation of hydrazine in an alkaline medium. The prepared catalysts with low Au loadings possess higher electroactivity towards the oxidation of hydrazine in an alkaline medium. Such behavior can be attributed to high dispersion of Au nanoparticles of high dispersity as well as alloy formation of Ni solid solution in gold [55]. Ghoshal *et al.* prepared multifunctional Pt-Nb composite by alloying of Nb with Pt. The tuned properties of Pt-Nb alloy made it a favorable electrocatalyst in multiple fuel cell systems [56]. In another study, the alloying effect improved the catalytic and electrochemical performance of CoPt/rGO catalyst which makes the process cost-effective [57]. An improvement in the activity of electrocatalysts has been reported for hydrazine electrooxidation by combining Co and noble metals such as Pt [58] or Pd [59], or Ni and noble metals [60], owing to large electrochemical surface area and high surface-to-volume ratio. Among these catalysts, CoPt NPs presented unique applications in the field of catalysis The synergistic effect between both metals resulted to the formation of alloy nanoparticles with high surface area, excellent catalytic activity, and high stability of the catalyst [61].

https://doi.org/10.1016/j.heliyon.2019.e01380
2405-8440/© 2019 Published by Elsevier Ltd. This is an open access article under the CC BY-NC-ND license (http://creativecommons.org/licenses/by-nc-nd/4.0/).

In electrode systems, supported bimetallic nanoparticles with high surface areas is important to improve and regulate the catalytic performances, to explore new electrode materials, and to find optimum compositions with efficient synergistic effects [62]. The activity of electrocatalyst depends on the size of the metal particles and their dispersion on the support. The requirements of an ideal support material include high surface area, optimum pore size distribution, good electrical conductivity, good physico-chemical stability, oxidative stability, and cost effectiveness [63]. Furthermore, a support offers the benefits of mass transport and electron transfer; all of these features contribute towards a superior catalytic efficiency [64]. Although, different carbon materials *i.e.,* carbon black, carbon nanotubes (CNTs), carbon nanofibers (CNFs), carbon nanowires (CNWs), and graphene have been applied as a catalytic support because of their large surface area, high electrical conductivity, and fine pore structures [65]. Among the earliest carbon-based supports, carbon black has been used extensively in fuel cell applications owing to its low cost, high availability and mesoporous distribution [66]. The carbon black should be activated before being used as a catalyst support to increase metal dispersion and its catalytic activity. However, several obstacles have been pointed for practical applications of carbon black, such as high temperature treatment for activation, insufficient electrochemical stability, low catalyst utilization due to poor mass transfer characteristics, diffusion limitation, and catalyst poisoning [67, 68]. Moreover, carbon black is also sensitive to electrochemical oxidation under many fuel cell service conditions such as H_2 starvation, under transient load and on/off operation, and a high cell potential, leading to carbon corrosion and detachment of metal NPs from the support material [69]. Advanced carbon materials (CNTs, CNFs, and CNWs) are also facing the major challenges to control their phase purity, crystal structure, and uniform dimensions during synthesis. There is also requirement of their functionalization prior to introduction of metal nanoparticles for improving metal dispersion and molecular interactions [70, 71].

In contrast, gamma alumina (γ-Al_2O_3) is an important catalyst support with a large surface area, pore volume, uniform pore-size distribution, mesoporous structure, good mechanical strength, and acid/base characteristics [72]. γ-Al_2O_3 is obtained by dehydration of aluminum hydroxide below 800 °C with controlled and reproducible properties [73]. Many electrochemical studies have shown that γ-Al_2O_3 adsorbed glassy carbon electrode can reduce the overpotential, enhance the rate of electrode reaction, and improve the sensitivity of several analytes due to the proton donating nature of oxide groups over the surface of alumina [74, 75, 76]. For electrochemical studies, an electrode provides both ionic and electronic conductivities. γ-Al_2O_3 and ZSM5 supported Sn catalysts were applied at cathode in electro-reduction cell in order to improve CO_2 conversion efficiency [77]. Since, γ-Al_2O_3 and ZSM5 supports are non-conducting in nature, the electronic conductivity may be delivered by inter connected metal nanoparticles present in the pore of the supports. The ionic

https://doi.org/10.1016/j.heliyon.2019.e01380
2405-8440/© 2019 Published by Elsevier Ltd. This is an open access article under the CC BY-NC-ND license (http://creativecommons.org/licenses/by-nc-nd/4.0/).

conductivity may be provided by electrolyte solution and Nafion ionomer used during preparation of catalyst slurry to coat the electrode. Lee et al. have successfully synthesized polyaniline/gamma aluminum oxide nanocomposites *via* in situ electropolymerization on gold electrodes (Au/PAn/γ-Al_2O_3) for the detection of vitamin E. The electrochemical performance of aniline in the presence of γ-Al_2O_3 nanoparticles enhanced dramatically [78]. Wang et al have deposited hexagonal γ -alumina nanosheets on carbon paste electrode for the electrocatalytic oxidation of alizarin [79]. No electrochemical response of alizarin was observed on a bare carbon paste electrode. However, nano γ -alumina catalyzes the electrochemical process of alizarin, especially the oxidation of alizarin very dramatically. The surface charge status and surface hydroxyl radical of γ -alumina are important factors in the electrocatalytic oxidation process.

The present work focused on the synthesis of γ-Al_2O_3 supported bimetallic $CoPt_x$ nanoalloys (x, Pt/Co molar ratio = 0, 0.017, 0.034, 0.048, 0.065, and 0.081) *via* wet impregnation method followed by H_2 reduction. Glassy carbon electrode was decorated with the synthesized catalyst material *via* drop casting technique and used as working electrode. The electro catalytic activity of the prepared catalysts was evaluated towards the oxidation of hydrazine in an alkaline medium using cyclic voltammetry technique. The morphology, structure, and composition of the prepared catalysts were studied by atomic absorption spectroscopy (AAS), X-ray diffraction (XRD), surface area analysis (SAA), scanning electron microscopy (SEM), energy dispersive X-ray spectroscopy (EDX), temperature programmed reduction (TPR), and temperature programmed oxidation (TPO).

2. Experimental

2.1. Materials

Aluminum chloride hexahydrate ($AlCl_3.6H_2O$, Panreac, 99.9%), ammonium hydroxide (NH_4OH, Fisher, 35%), cobalt acetate tetrahydrate (Co $(C_2H_3O_2)_2.4H_2O$, Merck, 99.9%), chloroplatinic acid hydrate ($H_2PtCl_6.xH_2O$, Aldrich, ~38% Pt basis) and hydrazine monohydrate ($N_2H_4.H_2O$, Panreac, 80%) were used as received without any purification. Deionized (DI) water with the ionic conductivity $\leq$3 μS cm^{-1} was used in the preparation of all aqueous solutions.

2.2. Catalyst preparation

At first, γ-Al_2O_3 support was prepared using aluminum chloride hexahydrate and ammonium hydroxide precursors by sol gel method as described in our previous work [80] and was fabricated in granular shape by adopting well established oil drop method [81]. The use of granular alumina support is practically beneficial for the facile transport of reactants and products. Bimetallic $CoPt_x/\gamma$-Al_2O_3 catalysts

https://doi.org/10.1016/j.heliyon.2019.e01380
2405-8440/© 2019 Published by Elsevier Ltd. This is an open access article under the CC BY-NC-ND license (http://creativecommons.org/licenses/by-nc-nd/4.0/).

were prepared by wet impregnation method. Prior to metal coating, γ-Al_2O_3 granules were oven dried at 120 °C for 2 h. During impregnation, γ-Al_2O_3 granules were immersed at first in aqueous solution of cobalt acetate for 1 h and subsequently, in chloroplatinic acid solution at room temperature for 1 h. The concentration of both metal solutions and impregnation steps were adjusted in such a manner to obtain the required stoichiometric ratio of Co and Pt metals. The use of multiple impregnations with dilute metal salt solution is beneficial to obtain the small size metal particles and good metal dispersion which ultimately results in superior catalytic activity [82]. After each metal coating, the catalysts were dried at room temperature for 2 h and then calcined at 550 °C for 4 h. Finally, the reduction was performed in a self-designed reactor equipped with programmable furnace, temperature controller, and H_2 gas flow meter. Prior to reduction, catalysts were dried under vacuum (~50 mbar) at 100 °C for 2h in the reactor. After that, reduction was initiated by passing H_2 gas (99.999% pure) at a flow rate of 20 cc/min and temperature was raised to 550 °C at the rate of 15 °C/min. The reduction process was continued for 4 h. The prepared catalysts were physically characterized by AAS, XRD, SEM, EDX, BET, TPR and TPO analyses to ensure the elemental composition, crystal structure, morphology, surface properties, and synergistic effect between Co and Pt metals to form Co-Pt alloy nanoparticles.

2.3. Electrode modification

The electrode modification was performed in various steps as schemed in Fig. 1. Prior to modification, bare glassy carbon electrode (GCE) was polished to a mirror finish on a felt pad using alumina powder (0.3 μm) and rinsed thoroughly with deionized water. The electrode was further ultra-sonicated in DI water for 5 min to remove any free alumina particles and was later dried at room temperature. The catalyst was grinded into fine powder and 0.1 mg of this powder was dispersed in 0.5 mL ethanol *via* ultra-sonication for 5 min. Simply, bare GCE (0.07 cm^2 surface area) was modified by introducing 2 μL of catalyst/ethanol dispersion, followed by drop casting of 2 μL of 0.5% Nafion solution. The electrode was dried at room temperature for 15 min, followed by oven drying at 60 °C for 30 min. All electrodes

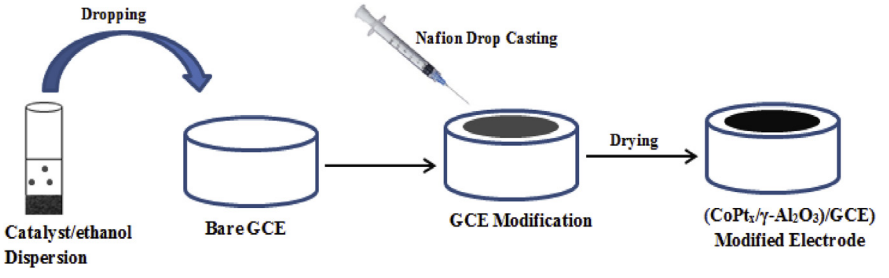

Fig. 1. Stepwise procedure for the electrode modification.

https://doi.org/10.1016/j.heliyon.2019.e01380
2405-8440/© 2019 Published by Elsevier Ltd. This is an open access article under the CC BY-NC-ND license (http://creativecommons.org/licenses/by-nc-nd/4.0/).

were modified in a similar manner. The modified electrodes ($CoPt_x/\gamma$-Al_2O_3)/GCE) were used for acquiring the electrochemical data of hydrazine oxidation. In order to reduce the background current, pre-conditioning was done in 20 cycles before each measurement in a respective potential window (0.5 V- 1.0 V) at the scan rate of 25 mV s^{-1}.

2.4. Characterization

The metal composition of the prepared catalysts was analyzed using atomic absorption spectroscopy (AAS) on Perkin Elmer AA400 atomic absorption spectrophotometer. For sample preparation, the catalyst was fused with sodium peroxide and potassium hydroxide mixture (1:1 ratio) at 600 °C and then dissolved in aqua regia. X-ray diffraction (XRD) patterns were recorded on PANalytical X'Pert Pro X-ray diffractometer for the identification of crystalline phases by using Cu Kα radiations ($\lambda = 0.154$ nm) in 2θ range of 20^o-80^o at scan rate of 0.04 θ s^{-1}. Surface area analysis was performed on Sorptometer Kelvin 1042 (Costech Instruments) at liquid N_2 temperature (−196 °C). Prior to each measurement, the sample was degassed at 200 °C for 2 h to remove moisture and physisorbed impurities. The surface morphology of the prepared catalysts was examined by MIRA3 (Tescan) scanning electron microscope (SEM) equipped with energy dispersive X-ray spectroscopy (EDX) unit. Temperature programmed reduction (TPR) measurements were performed on Chemisorb 2750 (Micromeritics) to evaluate Co and Al oxides phases and to ensure alloying effecting between Pt and Co metals. Prior to each TPR measurement, the pretreatment was performed by its activation in 10% O_2/He gas mixture at 200 °C for 4 h. Then sample was flushed with Ar gas for 2 h and cooled to room temperature. During TPR measurement, 10% H_2/He gas mixture was passed over the sample till to stable base line. The flow of reactive gas mixture was continued and temperature was raised from ambient up to 900 °C @ 15 °C min^{-1}. Finally, a plot of temperature versus thermal conductivity detector (TCD) signal was obtained. Temperature programmed oxidation (TPO) measurements were performed following TPR on Chemisorb 2750 (Micromeritics). After pretreatment of sample, the flow of 10% O_2/He gas mixture was passed over the sample and temperature was raised to 900 °C @ 15 °C min^{-1}. Finally, a plot of temperature versus TCD signal was obtained.

The electrochemical experiments were carried out at room temperature using potentiostat Interface1000 (Gamry Instruments) coupled with standard three electrode cell system consisting of modified GCE as working electrode, a platinum wire (dia: 0.5 mm) as an auxiliary electrode, and a saturated Ag/AgCl electrode (3 M KCl) as reference electrode. N_2H_4 solution was selected as analyte and phosphate buffer solution (PBS) was used as supporting electrolyte. 0.5 M N_2H_4 stock solution was prepared and was further diluted with PBS to make working solutions (*i.e.* 2 mM, 4 mM, 6

https://doi.org/10.1016/j.heliyon.2019.e01380
2405-8440/© 2019 Published by Elsevier Ltd. This is an open access article under the CC BY-NC-ND license (http://creativecommons.org/licenses/by-nc-nd/4.0/).

mM, 8 mM, and 10 mM). 0.1 M PBS was prepared by mixing equi-molar K_2HPO_4 and KH_2PO_4 solutions. All solutions were prepared in freshly DI water and CV measurements were performed in the potential window of 0.5−1.0 V.

3. Results and discussion

3.1. Composition and XRD analysis

The chemical composition of the prepared catalysts was determined by AAS and results are summarized in Table 1. AAS results were found relatively close to the theoretical metal contents in the prepared catalysts indicating the effectiveness of adapted procedures for incorporation of these metal phases together.

XRD patterns of pure γ-Al_2O_3 and $CoPt_x/\gamma$-Al_2O_3 catalysts are shown in Fig. 2. The cubic crystalline structure of γ-Al_2O_3 is confirmed by the appearance of its significant peaks at $2\theta \sim 37.6^o$, 45.8^o, and 66.7^o corresponding to (311), (400), and (440) hkl values, respectively, (ICDD Card No 00-001-1303). XRD pattern of monometallic Co/γ-Al_2O_3 catalyst presented two peaks of Co at 2θ values $\sim 30.1^\circ$ and 59.63° corresponding to (202) and (411) hkl values (ICDD Card No 01-070-2633). In contrast, XRD patterns of $CoPt_x/\gamma$-Al_2O_3 bimetallic catalysts depicted no prominent diffraction peaks of Pt metal which might be either due to low Pt contents or too small particles that cannot be detected [33]. Moreover, the diffraction peak of Co at 2θ value $\sim 30.1^o$ was noticed to shift towards the lower angle with an increase in Pt molar fraction which might be due to substitution of larger Pt atoms for the smaller Co atoms. This diffraction shift also indicated the formation of Co-Pt alloy NPs [83, 84].

Table 1. The elemental composition of $CoPt_x/\gamma$-Al_2O_3 bimetallic catalysts from AAS.

Samples	Co_{exp}[a] (wt%)	Pt_{exp}[b] (wt%)	Pt/Co[c]	M_{exp}[d] (wt%)	M_{th}[e] (wt%)	% Error[f]
Co/γ-Al_2O_3	18.92	0	0	18.92	20	5.4
$CoPt_{0.017}/\gamma$-Al_2O_3	19.10	1.07	0.017	20.17	21	3.95
$CoPt_{0.034}/\gamma$-Al_2O_3	18.99	2.13	0.034	21.12	22	4.0
$CoPt_{0.048}/\gamma$-Al_2O_3	19.22	3.05	0.048	22.27	23	3.17
$CoPt_{0.065}/\gamma$-Al_2O_3	18.95	4.11	0.065	23.06	24	3.92
$CoPt_{0.081}/\gamma$-Al_2O_3	19.15	5.12	0.081	24.27	25	2.92

[a] Co metal content determined by AAS.
[b] Pt metal content determined by AAS.
[c] Pt/Co molar ratio from experimental metal contents.
[d] Total experimental metal content.
[e] Total theoretical metal content.
[f] % error in theoretical and experimental results.

https://doi.org/10.1016/j.heliyon.2019.e01380
2405-8440/© 2019 Published by Elsevier Ltd. This is an open access article under the CC BY-NC-ND license (http://creativecommons.org/licenses/by-nc-nd/4.0/).

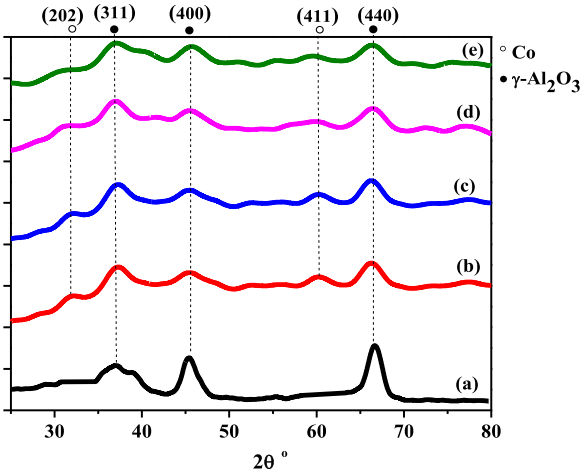

Fig. 2. XRD patterns of (a) γ-Al_2O_3 support, (b) Co/γ-Al_2O_3, (c) $CoPt_{0.017}$/γ-Al_2O_3, (d) $CoPt_{0.034}$/γ-Al_2O_3, and (e) $CoPt_{0.065}$/γ-Al_2O_3 catalysts.

3.2. Surface area analysis

In order to evaluate the specific surface area of the prepared $CoPt_{0.034}$/γ-Al_2O_3 catalyst, the N_2 adsorption and desorption measurements are further employed (Fig. 3a). According to the IUPAC classification, a typical type IV isotherm with a type H3 hysteresis loop at a relative pressure of 0.6−0.9 reveals the mesoporous nature of the material [85, 86]. Specific surface area of $CoPt_{0.034}$/γ-Al_2O_3 was calculated by the BET method and found to be 123 $m^2\ g^{-1}$ which is lower than bare γ-Al_2O_3 support (195 $m^2\ g^{-1}$). Such behavior can be ascribed to either filling of support pores with metal particles during impregnation or sintering of pores at high temperature treatment [87]. The pore size distribution of $CoPt_{0.034}$/γ-Al_2O_3 catalyst (Fig. 3b) was derived from the desorption isotherm using the Barret-Joyner-Halenda (BJH) method. Narrow pore size distribution of the catalyst was obtained with maxima centered at 4.68 nm reflecting a unimodal distribution of mesopores. All these observations indicated the textural difference in the properties of support after metal loadings.

3.3. SEM and EDX analyses

Fig. 4 presents the morphological features of the prepared catalysts as investigated by SEM. The loading of bimetallic CoPt nanoparticles resulted in the appearance of spherical particles over the surface of γ-Al_2O_3 substrate and they varied in size from 50 to 70 nm in diameter. Among homologues, $CoPt_{0.034}$/γ-Al_2O_3 catalyst displayed the uniform distribution and low agglomeration of CoPt alloy nanoparticles. High metal dispersion of this optimal catalyst resulted to a better catalytic activity for hydrazine electrooxidation, later on.

https://doi.org/10.1016/j.heliyon.2019.e01380
2405-8440/© 2019 Published by Elsevier Ltd. This is an open access article under the CC BY-NC-ND license (http://creativecommons.org/licenses/by-nc-nd/4.0/).

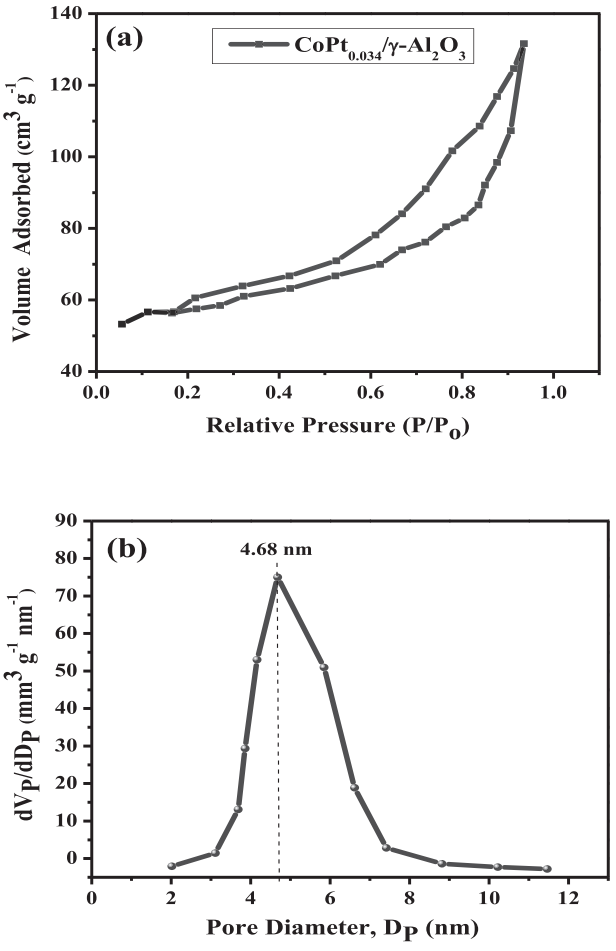

Fig. 3. N_2 adsorption-desorption isotherm and (b) pore size distribution curve of $CoPt_{0.034}/\gamma\text{-}Al_2O_3$ catalyst using BJH method.

The elemental composition of $CoPt_x/\gamma\text{-}Al_2O_3$ bimetallic catalysts was further confirmed by EDX analysis as shown in Fig. 5(a-d). The co-existence of Co and Pt metals in EDX patterns illustrated the synergistic effect of Co and Pt metals to form Co-Pt alloy NPs over the surface of Al_2O_3 support. EDX results for $CoPt_x/\gamma\text{-}Al_2O_3$ catalysts are listed in Table 2 that were found in good agreement with AAS results thus confirming the stoichiometric metal contents.

Moreover, EDX mapping (Fig. 5e) of $CoPt_{0.034}/\gamma\text{-}Al_2O_3$ catalyst showed a uniform distribution of Co and Pt along with the constitution elements of support (Al and O).

3.4. TPR and TPO measurements

The profiles obtained in the TPR tests of catalysts are shown in Fig. 6a. In accordance with earlier reports [88, 89] monometallic $Co/\gamma\text{-}Al_2O_3$ catalyst presented peaks in three regions *i.e.,* first peak at 150 °C, second peak at 200 °C and third broad

https://doi.org/10.1016/j.heliyon.2019.e01380
2405-8440/© 2019 Published by Elsevier Ltd. This is an open access article under the CC BY-NC-ND license (http://creativecommons.org/licenses/by-nc-nd/4.0/).

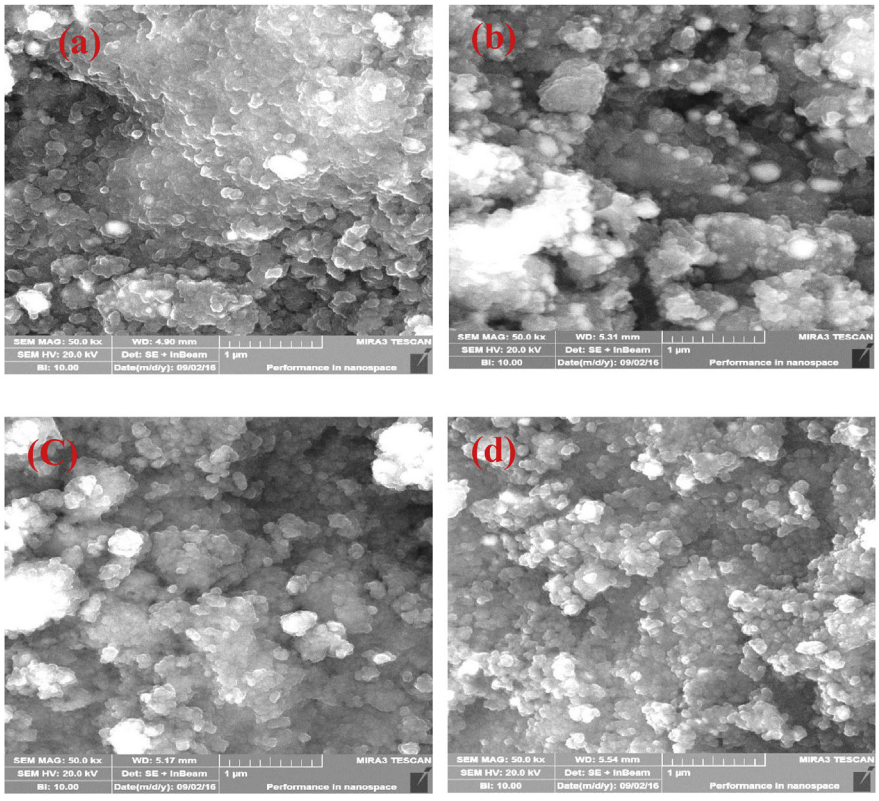

Fig. 4. SEM images of prepared catalysts: (a) $CoPt_{0.017}/\gamma\text{-}Al_2O_3$, (b) $CoPt_{0.034}/\gamma\text{-}Al_2O_3$, (c) $CoPt_{0.048}/\gamma\text{-}Al_2O_3$, and (d) $CoPt_{0.081}/\gamma\text{-}Al_2O_3$.

peak around 400 °C. The first peak appeared for a complete decomposition of the cobalt precursor and its intensity greatly diminishes by prolonged calcination [90]. The second peak was ascribed to the transformation of Co_3O_4 to CoO, while broad band appeared upon complete reduction of Co_3O_4 to Co^0 [91]. A broad band was observed at 600 °C which corresponds to the reduction of cobalt aluminates ($CoAl_2O_4$) spinal [92, 93]. Batley *et al.* for the first time showed the influence of Pt atoms on Co reduction [94]. More recently, Holmen and coworkers illustrated high effect of Pt atoms on Co reducibility especially, for alumina supported catalysts [95, 96]. The TPR profiles of all the bimetallic catalysts exhibited three peaks of hydrogen consumption. The first and the third peaks, assigned to the reduction of cobalt species, are still observed at the same temperature as in the monometallic Co catalyst. For bimetallic $CoPt_x/\gamma\text{-}Al_2O_3$ catalysts, the second peak at 350 °C was assigned to the reduction of cobalt oxides in intimate interaction with Pt. The appearance of this peak indicated the formation of CoPt alloy phase. Moreover, with an increase in Pt loadings, this peak was shifted slightly towards lower temperatures. These results suggest the influence of Pt in lowering the reduction temperature of cobalt species and also decreasing the interaction of the metallic species with the support.

https://doi.org/10.1016/j.heliyon.2019.e01380
2405-8440/© 2019 Published by Elsevier Ltd. This is an open access article under the CC BY-NC-ND license (http://creativecommons.org/licenses/by-nc-nd/4.0/).

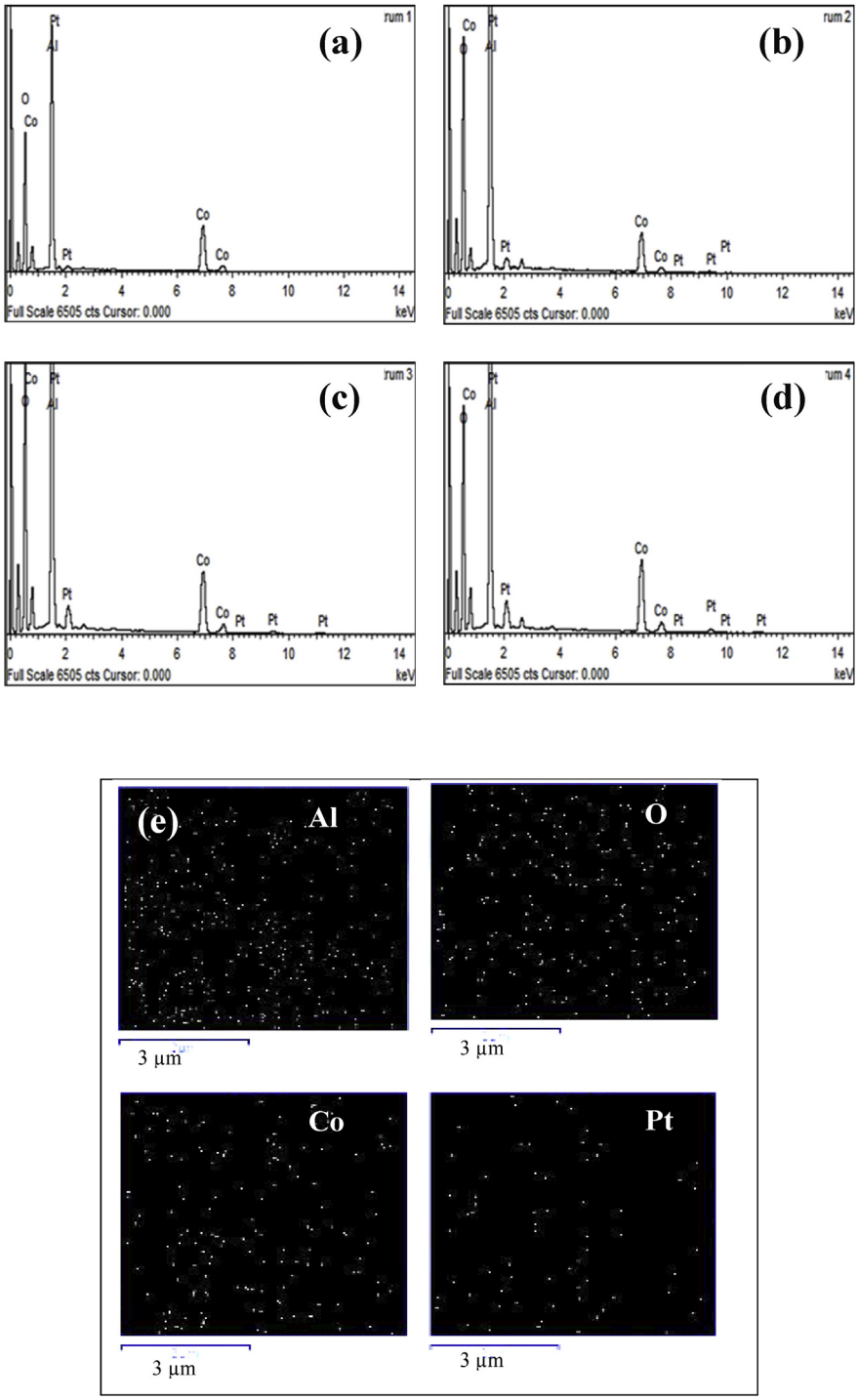

Fig. 5. EDX profiles of (a) $CoPt_{0.017}/\gamma\text{-}Al_2O_3$, (b) $CoPt_{0.034}/\gamma\text{-}Al_2O_3$, (c) $CoPt_{0.065}/\gamma\text{-}Al_2O_3$, and (d) $CoPt_{0.081}/\gamma\text{-}Al_2O_3$, and (e) EDX mapping of $CoPt_{0.034}/\gamma\text{-}Al_2O_3$ catalyst.

https://doi.org/10.1016/j.heliyon.2019.e01380
2405-8440/© 2019 Published by Elsevier Ltd. This is an open access article under the CC BY-NC-ND license (http://creativecommons.org/licenses/by-nc-nd/4.0/).

Table 2. The elemental composition of $CoPt_x/\gamma\text{-}Al_2O_3$ bimetallic catalysts from EDX analysis.

Catalyst	Wt% O	Wt% Al	Wt% Co	Wt% Pt
$CoPt_{0.017}/\gamma\text{-}Al_2O_3$	42.53	35.73	19.90	1.84
$CoPt_{0.034}/\gamma\text{-}Al_2O_3$	44.68	34.69	18.38	2.25
$CoPt_{0.048}/\gamma\text{-}Al_2O_3$	41.68	34.64	20.22	3.46
$CoPt_{0.065}/\gamma\text{-}Al_2O_3$	40.52	34.37	20.58	4.53
$CoPt_{0.081}/\gamma\text{-}Al_2O_3$	41.57	33.71	18.94	5.78

Fig. 6b shows the TPO profiles of monometallic and bimetallic catalysts. $Co/\gamma\text{-}Al_2O_3$ catalyst showed an oxidation band at 200−450 °C, attributing to the oxidation of Co to Co_3O_4. No oxidation peak was observed for cobalt aluminates indicating their difficult oxidation, once they have been formed. The oxidation peak for the $CoPt_x/\gamma\text{-}Al_2O_3$ catalysts, was shifted to a lower temperature range upon incorporation of Pt loadings. This shift in peak position could be ascribed to the synergistic effect of Co and Pt metals to form CoPt nanoalloys.

3.5. Electrooxidation of hydrazine on modified electrodes

To investigate the electrochemical oxidation of hydrazine, cyclic voltammograms at bare GCE and $Co/\gamma\text{-}Al_2O_3$ modified GCE were recorded (Fig. 7). Both electrodes presented no oxidation peak. For comparative studies, electrocatalytic oxidation of hydrazine was tested with $CoPt_x/\gamma\text{-}Al_2O_3$ modified GCE with different molar ratios of Pt. CV profiles of these modified electrodes presented a positive shift of the oxidation potential as well as an enhancement of anodic current. All the modified electrodes showed an ability to oxidize hydrazine. The greatest current response was noticed for $CoPt_{0.034}/\gamma\text{-}Al_2O_3$ catalyst with anodic peak current (i_P) value of 200 μA at ~0.87 V. This anodic peak results from the electrode reaction of:

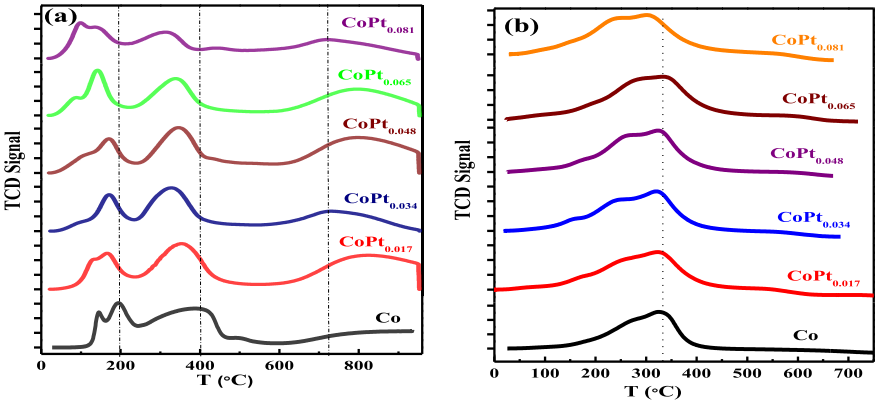

Fig. 6. (a) TPR and (b) TPO profiles of the prepared materials.

https://doi.org/10.1016/j.heliyon.2019.e01380
2405-8440/© 2019 Published by Elsevier Ltd. This is an open access article under the CC BY-NC-ND license (http://creativecommons.org/licenses/by-nc-nd/4.0/).

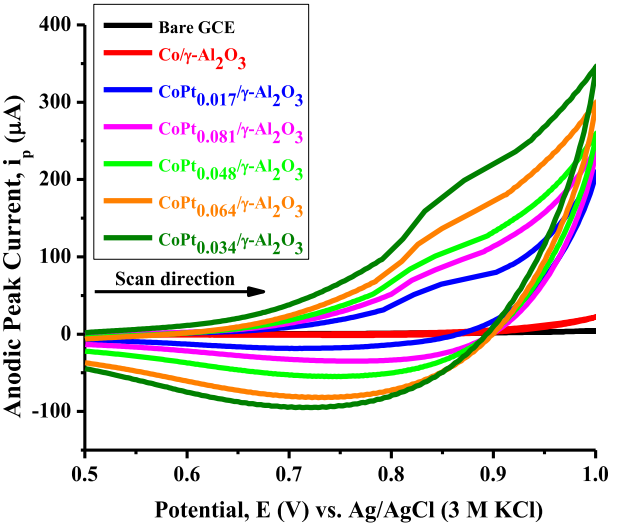

Fig. 7. CV profiles of bare GCE and $CoPt_x/\gamma$-Al_2O_3 modified GCE in 2 mM N_2H_4 using 0.1 M PBS (pH 7.2) at 25 mV s^{-1}.

$N_2H_4 \rightarrow N_2 + 4H^+ + 4e^-$. Bimetallic modified GCE showed a highest current response, than monometallic Co modified GCE. An increase in the oxidation peak current shows the better electrochemical efficiency of this electrode towards hydrazine oxidation, which is attributable to high surface area and facile electron transfer ability [97].

3.6. Effect of scan rate

To examine the voltammetric behavior of the modified electrode, hydrazine elctrooxidation was performed by changing the scan rate in the range of 10−100 mV s^{-1} and results are shown in Fig. 8a. The resultant oxidation current was observed *via* cyclic voltammetry in 0.1 M PBS solution (pH 7.2) containing 2 mM hydrazine. The anodic peak current was observed to increase with increasing the scan rates. A linear relationship was obtained by plotting anodic peak current (i_p) as a function of scan rate (Fig. 8b). The linear regression equation is as follows:

$$i_p\ (\mu A) = 429.3\ (\upsilon)^{1/2} - 7.4\ (R^2 = 0.99) \quad (3)$$

This linear trend proved that the electrochemical process on the modified electrode was controlled by surface adsorption. Moreover, the linear dependence of peak current on the scan rate (Fig. 8c), further confirmed the diffusion character of hydrazine electrooxidation as designated by following equation [98, 99].

$$\ln i_p = 0.5403\ \ln\upsilon\ (\text{V s}^{-1}) + 6.10\ (R^2 = 0.99) \quad (4)$$

https://doi.org/10.1016/j.heliyon.2019.e01380
2405-8440/© 2019 Published by Elsevier Ltd. This is an open access article under the CC BY-NC-ND license (http://creativecommons.org/licenses/by-nc-nd/4.0/).

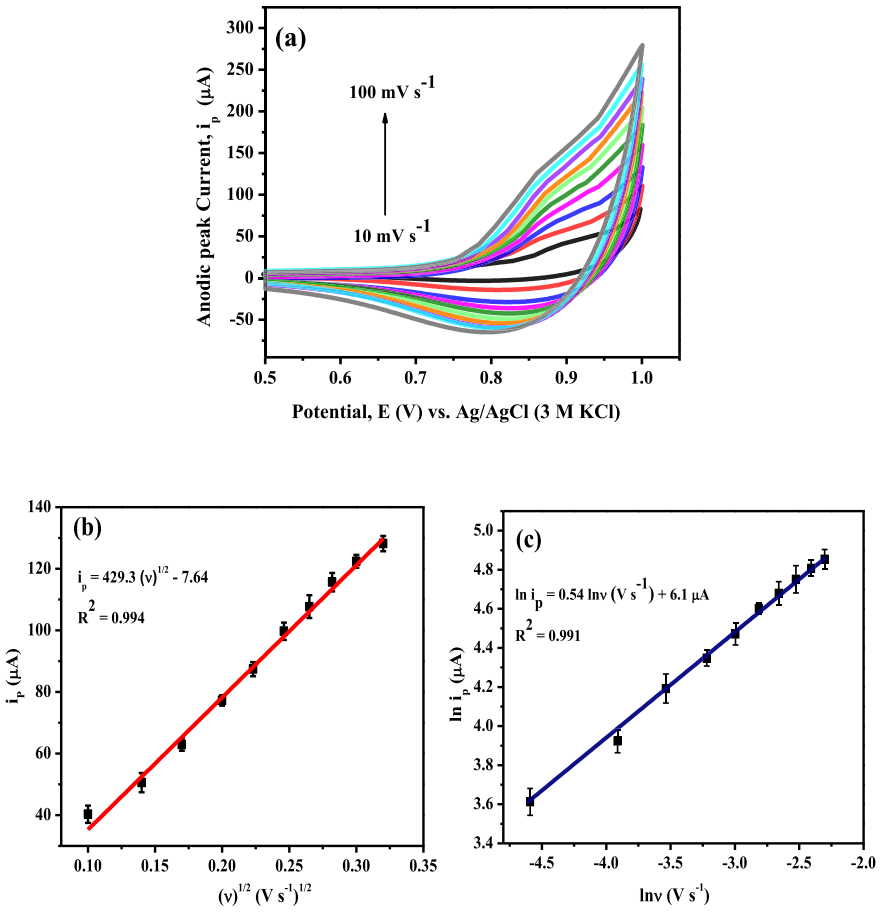

Fig. 8. (a) Cyclic voltammetric profiles of modified electrode at scan rate of 10−100 mV s^{-1}, (b) dependence of anodic peak current on $\nu^{1/2}$, and (c) linear dependence of peak current on scan rate (both in logarithm scales).

3.7. Effect of hydrazine concentration

The effect of hydrazine concentration on oxidation peak current for $CoPt_{0.034}/\gamma$-Al_2O_3 modified GCE in 0.1 M PBS (pH 7.2) is shown in Fig. 9a. The hydrazine concentration was varied from 2 to 10 mM. The anodic peak current was found proportional to hydrazine concentration which can be correlated to the better distribution of bimetallic alloy NPs over the surface of this modified electrode [100]. The current response was found linear to N_2H_4 concentration with a correlation coefficient of 0.996 as shown in Fig. 9b.

The comparison of electroanalytical data of our modified electrodes with reported ones for hydrazine oxidation is listed in Table 3.

The peak current response of our modified electrode is higher as compared to other reported modified electrodes for hydrazine electrooxidation. This robust performance can be correlated to the synergistic effect between Co and Pt metals, high

https://doi.org/10.1016/j.heliyon.2019.e01380
2405-8440/© 2019 Published by Elsevier Ltd. This is an open access article under the CC BY-NC-ND license (http://creativecommons.org/licenses/by-nc-nd/4.0/).

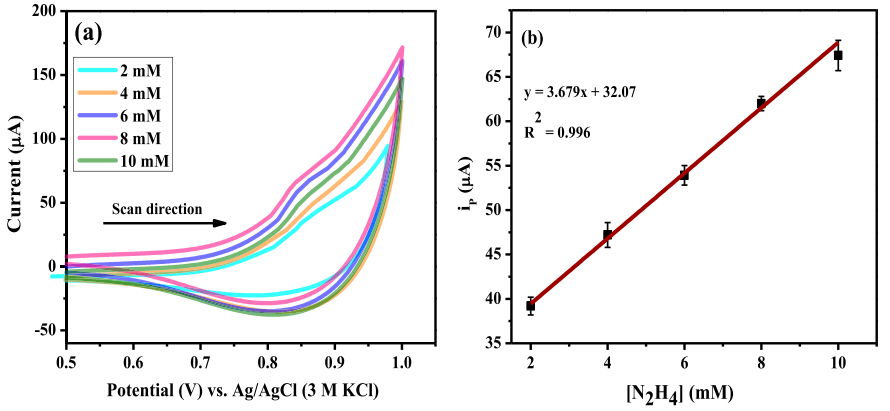

Fig. 9. (a) Effect of N_2H_4 concentration (2−10 mM) for $CoPt_{0.034}/\gamma$-Al_2O_3 modified electrode in 0.1 M PBS (pH 7.2) at 25 mV s^{-1} and (b) a plot of i_P versus N_2H_4 concentration.

dispersion of CoPt alloy particles, small-sized particles, improved reducibility, and presence of more active sites as confirmed by XRD, SEM, TEM, EDX, and TPR/TPO analyses.

3.8. Reproducibility and stability studies

The reproducibility and stability of the $CoPt_{0.034}/\gamma$-Al_2O_3/GCE were investigated by CV method in 10 successive runs using 2 mM hydrazine. Fig. 10a shows that CV response of the modified electrode was maintained in all cycles with a relative standard deviation (RSD) of 2.86%, indicating its good repeatability and stability. The stability of projected electrocatalysts was evaluated on the basis of reproducible current response for five identical electrodes using $CoPt_{0.034}/\gamma$-Al_2O_3. Anodic peak current output for 2 mM hydrazine is represented as a bar chart in Fig. 10b. Only a little

Table 3. Comparison of electroanalytical performance of our modified electrodes with reported catalysts for electrooxidation of hydrous hydrazine.

Electrode type	N_2H_4 Conc.	Electrolyte	Scan rate (mV s^{-1})	Peak potential (V)	Anodic peak current	Ref.
Au/SWCNHs/GCE	0.3 mM	0.1 M PBS (pH 7.4)	25	0.26	13 μA	[35]
G/NiCuCo	0.4 M	0.1 M NaOH	100	0.70	53 mA cm^{-2}[a]	[36]
NGPVP/AuNPs/SPCE	0.5 mM	0.1 M PBS (pH 7)	100	0.003	80 μA	[38]
Au-Cu/NPZ/CPE	9 mM	0.1 M PBS (pH 7.4)	50	0.20	5 mA cm^{-2}[a]	[53]
Au-Pd NP/GNP/GCE	0.1 mM	0.1 M PBS (pH 6)	10	0.53	60 μA	[54]
Au(Ni)/TiO_2-NTs	0.05 M	1 M NaOH	10	-1.0	60 mA cm^{-2}[a]	[55]
PdNPs-EDAC/GCE	50 μM	0.1 M PBS (pH 7)	50	−0.05	4 μA	[44]
NiO_x-Pt/C	0.1 M	1 M KOH	25	0.20	30 mA cm^{-2}[a]	[60]
($CoPt_{0.034}/\gamma$-Al_2O_3)/GCE	**2 mM**	0.1 M PBS (pH 7.2)	**25**	**0.85**	**183.2 μA**	**This work**

[a] Current density values are given in column 6 for references [33, 36, 46, 60].

https://doi.org/10.1016/j.heliyon.2019.e01380
2405-8440/© 2019 Published by Elsevier Ltd. This is an open access article under the CC BY-NC-ND license (http://creativecommons.org/licenses/by-nc-nd/4.0/).

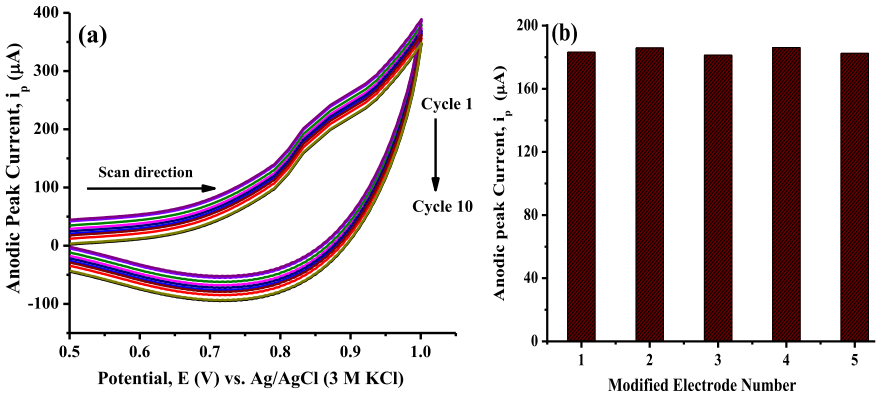

Fig. 10. (a) CV profiles of $CoPt_{0.034}/\gamma$-Al_2O_3 modified GCE in 10 successive cycles for hydrazine electrooxidation in 0.1 M PBS (pH 7.2) at 25 mV s^{-1} and (b) anodic peak current response of five identical ($CoPt_{0.034}/\gamma$-Al_2O_3)/GCE in 2 mM N_2H_4.

variation was observed in the anodic current responses of five identical electrodes. The average anodic peak current on the modified electrodes and relative standard deviation (RSD) are 183.8 μA and 2.45% respectively suggesting a good reproducibility of the prepared electrodes.

4. Conclusions

In conclusion, advanced materials, $CoPt_x/\gamma$-Al_2O_3 were synthesized by wet impregnation method. All catalysts presented good mechanical and chemical stability. These materials proved electro-catalytically active towards hydrazine oxidation in an alkaline environment. The combination of Co with Pt improved the material's properties in a way that the overpotential for the hydrazine oxidation was greatly reduced in comparison to Co/γ-Al_2O_3. The synergistic effect for the formation of CoPt nanoalloys was advantageous for electrochemical process of hydrazine oxidation. All catalysts responded for the hydrazine electrooxidation with maximum anodic current for $CoPt_{0.034}/\gamma$-Al_2O_3 catalyst. Hence, $CoPt_{0.034}/\gamma$-Al_2O_3 was established as an optimal composition due to its prominent electrocatalytic response. The prominent electrochemical response towards hydrazine electrooxidation indicated that these materials may further contribute to applications in the field of catalysis, electroanalysis, and sensing.

Declarations

Author contribution statement

Naveeda Firdous, Naveed K. Janjua: Conceived and designed the experiments; Performed the experiments; Analyzed and interpreted the data; Contributed reagents, materials, analysis tools or data; Wrote the paper.

https://doi.org/10.1016/j.heliyon.2019.e01380
2405-8440/© 2019 Published by Elsevier Ltd. This is an open access article under the CC BY-NC-ND license (http://creativecommons.org/licenses/by-nc-nd/4.0/).

Funding statement

This research did not receive any specific grant from funding agencies in the public, commercial, or not-for-profit sectors.

Competing interest statement

The authors declare no conflict of interest.

Additional information

Data associated with this study has been deposited at HEC Pakistan. The repository link is here: http://prr.hec.gov.pk/jspui/handle/123456789/9060.

Acknowledgements

Quaid-i-Azam University Islamabad is highly acknowledged for lab research facility. We acknowledge Institute of Space Technology Islamabad for SEM and EDX analyses. We also acknowledge Pakistan Institute Engineering & Applied Sciences Islamabad for TPR and TPO measurements. HEC Pakistan is acknowledged for the funding from 20-1718 and 14-4768 Projects.

References

[1] M. Zheng, Y. Zhou, Y. Chen, Y. Tang, T. Lu, Electrochemical behavior of dopamine in the presence of phosphonate and the determination of dopamine at phosphonate modified zirconia films electrode with highly antifouling capability, Electrochim. Acta 55 (2010) 4789−4798.

[2] E.W. Schmidt, Hydrazine and its Derivatives, Wiley-Interscience, 2001.

[3] J.K. Morris, N.J. Wald, A.L. Springett, Occupational exposure to hydrazine and subsequent risk of lung cancer: 50-year follow-up, PLoS One 10 (2015) 1−6.

[4] I.C. Vieira, K.O. Lupetti, O. Fatibello-Filho, Sweet potato tissue as a biocatalyst in a paraffin/graphite biosensor for hydrazine determination in boiler feed water, Anal. Lett. 35 (2002) 2221−2231.

[5] J. Schirmann, P. Bourdauducq, in: Hydrazine. Ullmann's Encyclopedia of Industrial Chemistry, Wiley-VCH, Weinheim, 2002.

[6] P. Zhao, N. Cao, J. Su, W. Luo, G. Cheng, NiIr nanoparticles immobilized on the pores of MIL-101 as highly efficient catalyst toward hydrogen generation from hydrous hydrazine, ACS Sustain. Chem. Eng. 3 (2015) 1086−1093.

https://doi.org/10.1016/j.heliyon.2019.e01380
2405-8440/© 2019 Published by Elsevier Ltd. This is an open access article under the CC BY-NC-ND license (http://creativecommons.org/licenses/by-nc-nd/4.0/).

[7] H.L. Wang, J.M. Yan, Z.L. Wang, O. Song Il, Q. Jiang, Highly efficient hydrogen generation from hydrous hydrazine over amorphous $Ni_{0.9}Pt_{0.1}$/Ce_2O_3 nanocatalyst at room temperature, J. Mater. Chem. A 1 (2013) 14957−14962.

[8] O. Song-Il, J.M. Yan, H.L. Wang, Z.L. Wang, Q. Jiang, Ni/La_2O_3 catalyst containing low content platinum-rhodium for the dehydrogenation of $N_2H_4.H_2O$ at room temperature, J. Power Sources 262 (2014) 386−390.

[9] T. Liu, J. Yu, H. Bie, Z. Hao, Highly efficient hydrogen generation from hydrous hydrazine using a reduced graphene oxide-supported NiPtP nanoparticle catalyst, J. Alloys Comp. 690 (2017) 783−790.

[10] J. Chen, Z.-H. Lu, W. Huang, Z. Kang, X. Chen, Galvanic replacement synthesis of NiPt/graphene as highly efficient catalysts for hydrogen release from hydrazine and hydrazine borane, J. Alloys Comp. 695 (2017) 3036−3043.

[11] M. Ni, M.K. Leung, D.Y. Leung, Technological development of hydrogen production by solid oxide electrolyzer cell (SOEC), Int. J. Hydrogen Energy 33 (2008) 2337−2354.

[12] B. Chen, H. Xu, H. Zhang, P. Tan, W. Cai, M. Ni, A novel design of solid oxide electrolyser integrated with magnesium hydride bed for hydrogen generation and storage−a dynamic simulation study, Appl. Energy 200 (2017) 260−272.

[13] K. Yang, K. Yang, S. Zhang, Y. Luo, Q. Yao, Z.-H. Lu, Complete dehydrogenation of hydrazine borane and hydrazine catalyzed by MIL-101 supported NiFePd nanoparticles, J. Alloys Comp. 732 (2018) 363−371.

[14] R. Von Burg, T. Stout, Hydrazine, J. Appl. Toxicol. 11 (1991) 447−450.

[15] A. Umar, M. Rahman, Y.-B. Hahn, Ultra-sensitive hydrazine chemical sensor based on high-aspect-ratio ZnO nanowires, Talanta 77 (2009) 1376−1380.

[16] S. Amlathe, V. Gupta, Spectrophotometric determination of trace amounts of hydrazine in polluted water, Analyst 113 (1988) 1481−1483.

[17] M. George, K. Nagaraja, N. Balasubramanian, Spectrophotometric determination of hydrazine, Anal. Lett. 40 (2007) 2597−2605.

[18] M. Mori, K. Tanaka, Q. Xu, M. Ikedo, H. Taoda, W. Hu, Highly sensitive determination of hydrazine ion by ion-exclusion chromatography with ion-exchange enhancement of conductivity detection, J. Chromatogr. A 1039 (2004) 135−139.

https://doi.org/10.1016/j.heliyon.2019.e01380
2405-8440/© 2019 Published by Elsevier Ltd. This is an open access article under the CC BY-NC-ND license (http://creativecommons.org/licenses/by-nc-nd/4.0/).

[19] H.E. Malone, D. Anderson, The determination of mixtures of hydrazine, monomethyl-hydrazine and 1, 1-dimethylhydrazine, Anal. Chim. Acta 48 (1969) 87–91.

[20] M. Michlmayr, D.T. Sawyer, Electrochemical oxidation of hydrazine and of the dimethylhydrazines in dimethylsulfoxide at a platinum electrode, J. Electroanal. Chem. Interfacial Electrochem. 23 (1969) 375–385.

[21] W. Hou, H. Ji, E. Wang, Amperometric flow-injection analysis of hydrazine by electrocatalytic oxidation at cobalt tetraphenylporphyrin modified electrode with heat treatment, Talanta 39 (1992) 45–50.

[22] M. Koupparis, T. Hadjiioannou, Indirect potentiometric determination of hydrazine, isoniazid, sulphide and thiosulphate with a chloramine-T ion-selective electrode, Talanta 25 (1978) 477–480.

[23] S. Chakraborty, C.R. Raj, Carbon nanotube supported platinum nanoparticles for the voltammetric sensing of hydrazine, Sensor. Actuator. B Chem. 147 (2010) 222–227.

[24] A.A. Ensafi, E. Mirmomtaz, Electrocatalytic oxidation of hydrazine with pyrogallol red as a mediator on glassy carbon electrode, J. Electroanal. Chem. 583 (2005) 176–183.

[25] A. Abbaspour, M. Shamsipur, A. Siroueinejad, R. Kia, P.R. Raithby, Renewable-surface sol–gel derived carbon ceramic-modified electrode fabricated by a newly synthesized polypyridil and phosphine Ru (II) complex and its application as an amperometric sensor for hydrazine, Electrochim. Acta 54 (2009) 2916–2923.

[26] K. Ghanbari, Fabrication of silver nanoparticles–polypyrrole composite modified electrode for electrocatalytic oxidation of hydrazine, Synth. Met. 195 (2014) 234–240.

[27] M. Fleischmann, K. Korinek, D. Pletcher, The oxidation of hydrazine at a nickel anode in alkaline solution, J. Electroanal. Chem. Interfacial Electrochem. 34 (1972) 499–503.

[28] M. Petek, S. Bruckenstein, An isotopic labeling investigation of the mechanism of the electrooxidation of hydrazine at platinum: an electrochemical mass spectrometric study, J. Electroanal. Chem. Interfacial Electrochem. 47 (1973) 329–333.

[29] C. Zhang, G. Wang, Y. Ji, M. Liu, Y. Feng, Z. Zhang, B. Fang, Enhancement in analytical hydrazine based on gold nanoparticles deposited on ZnO-MWCNTs films, Sensor. Actuator. B Chem. 150 (2010) 247–253.

 https://doi.org/10.1016/j.heliyon.2019.e01380
2405-8440/© 2019 Published by Elsevier Ltd. This is an open access article under the CC BY-NC-ND license (http://creativecommons.org/licenses/by-nc-nd/4.0/).

[30] A.S. Kumar, R. Shanmugam, N. Vishnu, K.C. Pillai, S. Kamaraj, Electrochemical immobilization of ellagic acid phytochemical on MWCNT modified glassy carbon electrode surface and its efficient hydrazine electrocatalytic activity in neutral pH, J. Electroanal. Chem. 782 (2016) 215–224.

[31] J. Li, X. Lin, Electrocatalytic oxidation of hydrazine and hydroxylamine at gold nanoparticle—polypyrrole nanowire modified glassy carbon electrode, Sensor. Actuator. B Chem. 126 (2007) 527–535.

[32] R.C. Engstrom, Electrochemical pretreatment of glassy carbon electrodes, Anal. Chem. 54 (1982) 2310–2314.

[33] J.M. Zen, A.S. Kumar, D.M. Tsai, Recent updates of chemically modified electrodes in analytical chemistry, Electroanalysis 15 (2003) 1073–1087.

[34] H. Heli, M. Hajjizadeh, A. Jabbari, A. Moosavi-Movahedi, Fine steps of electrocatalytic oxidation and sensitive detection of some amino acids on copper nanoparticles, Anal. Biochem. 388 (2009) 81–90.

[35] S. Zhao, L. Wang, T. Wang, Q. Han, S. Xu, A high-performance hydrazine electrochemical sensor based on gold nanoparticles/single-walled carbon nanohorns composite film, Appl. Surf. Sci. 369 (2016) 36–42.

[36] M. Jafarian Hosseini, T. Rostami, M. Mahjani, F. Gobal, A low cost and highly active non-noble alloy electrocatalyst for hydrazine oxidation based on nickel ternary alloy at the surface of graphite electrode, J. Electroanal. Chem. 763 (2016) 134–140.

[37] F. Yang, K. Cheng, G. Wang, D. Cao, Flower-like Co nano-particles deposited on Ni foam substrate as efficient noble metal-free catalyst for hydrazine oxidation, J. Electroanal. Chem. 756 (2015) 186–192.

[38] C. Saengsookwaow, R. Rangkupan, O. Chailapakul, N. Rodthongkum, Nitrogen-doped graphene–polyvinylpyrrolidone/gold nanoparticles modified electrode as a novel hydrazine sensor, Sensor. Actuator. B Chem. 227 (2016) 524–532.

[39] K. Ravichandran, R.P. Baldwin, Liquid chromatographic determination of hydrazines with electrochemically pretreated glassy carbon electrodes, Anal. Chem. 55 (1983) 1782–1786.

[40] K.M. Korfhage, K. Ravichandran, R.P. Baldwin, Phthalocyanine-containing chemically modified electrodes for electrochemical detection in liquid chromatography/flow injection systems, Anal. Chem. 56 (1984) 1514–1517.

https://doi.org/10.1016/j.heliyon.2019.e01380
2405-8440/© 2019 Published by Elsevier Ltd. This is an open access article under the CC BY-NC-ND license (http://creativecommons.org/licenses/by-nc-nd/4.0/).

[41] J. Wang, P.V. Pamidi, C.L. Renschler, C. White, Metal-dispersed porous carbon films as electrocatalytic sensors, J. Electroanal. Chem. 404 (1996) 137−142.

[42] W. Zhou, L. Xu, M. Wu, L. Xu, E. Wang, Determination of hydrazines by capillary zone electrophoresis with amperometric detection at a platinum particle-modified carbon fibre microelectrode, Anal. Chim. Acta 299 (1994) 189−194.

[43] T. Li, E. Wang, Electrocatalytic oxidation and flow amperometric detection of hydrazine at an electropolymerized 4-vinylpyridine/palladium film electrode, Electroanalysis 9 (1997) 1205−1208.

[44] H. Ahmar, S. Keshipour, H. Hosseini, A.R. Fakhari, A. Shaabani, A. Bagheri, Electrocatalytic oxidation of hydrazine at glassy carbon electrode modified with ethylenediamine cellulose immobilized palladium nanoparticles, J. Electroanal. Chem. 690 (2013) 96−103.

[45] S.M. Golabi, F. Noor-Mohammadi, Electrocatalytic oxidation of hydrazine at cobalt hexacyanoferrate-modified glassy carbon, Pt and Au electrodes, J. Solid State Electrochem. 2 (1998) 30−37.

[46] C.M. Welch, R.G. Compton, The use of nanoparticles in electroanalysis: a review, Anal. Bioanal. Chem. 384 (2006) 601−619.

[47] L. Shaidarova, G. Budnikov, Chemically modified electrodes based on noble metals, polymer films, or their composites in organic voltammetry, J. Anal. Chem. 63 (2008) 922−942.

[48] M. Oyama, Recent nanoarchitectures in metal nanoparticle-modified electrodes for electroanalysis, Anal. Sci. 26 (2010) 1−12.

[49] B. Dong, B.-L. He, J. Huang, G.-Y. Gao, Z. Yang, H.-L. Li, High dispersion and electrocatalytic activity of Pd/titanium dioxide nanotubes catalysts for hydrazine oxidation, J. Power Sources 175 (2008) 266−271.

[50] M. Tominaga, Y. Taema, I. Taniguchi, Electrocatalytic glucose oxidation at bimetallic gold−copper nanoparticle-modified carbon electrodes in alkaline solution, J. Electroanal. Chem. 624 (2008) 1−8.

[51] D. Wang, Y. Li, Bimetallic nanocrystals: liquid-phase synthesis and catalytic applications, Adv. Mater. 23 (2011) 1044−1060.

[52] T. Sakamoto, K. Asazawa, J. Sanabria-Chinchilla, U. Martinez, B. Halevi, P. Atanassov, P. Strasser, H. Tanaka, Combinatorial discovery of Ni-based binary and ternary catalysts for hydrazine electrooxidation for use in anion exchange membrane fuel cells, J. Power Sources 247 (2014) 605−611.

https://doi.org/10.1016/j.heliyon.2019.e01380
2405-8440/© 2019 Published by Elsevier Ltd. This is an open access article under the CC BY-NC-ND license (http://creativecommons.org/licenses/by-nc-nd/4.0/).

[53] F. Amiripour, S.N. Azizi, S. Ghasemi, Gold-copper bimetallic nanoparticles supported on nano P zeolite modified carbon paste electrode as an efficient electrocatalyst and sensitive sensor for determination of hydrazine, Biosens. Bioelectron. 107 (2018) 111−117.

[54] Q. Wan, Y. Liu, Z. Wang, W. Wei, B. Li, J. Zou, N. Yang, Graphene nanoplatelets supported metal nanoparticles for electrochemical oxidation of hydrazine, Electrochem. Commun. 29 (2013) 29−32.

[55] Tamašauskaitė-Tamašiūnaitė, J. Rakauskas, A. Balčiūnaitė, A. Zabielaitė, J. Vaičiūnienė, A. Selskis, R. Juškėnas, V. Pakštas, E. Norkus, Gold−nickel/titania nanotubes as electrocatalysts for hydrazine oxidation, J. Power Sources 272 (2014) 362−370.

[56] S. Ghoshal, Q. Jia, M.K. Bates, J. Li, C. Xu, K. Gath, J. Yang, J. Waldecker, H. Che, W. Liang, Tuning Nb-Pt interactions to facilitate fuel cell electrocatalysis, ACS Catal. 7 (2017) 4936−4946.

[57] M. Sevim, C. Francia, J. Amici, S. Vankova, T. Sener, O. Metin, Bimetallic MPt (M: Co, Cu, Ni) alloy nanoparticles assembled on reduced graphene oxide as high performance cathode catalysts for rechargable lithium-oxygen batteries, J. Alloy. Comp. 683 (2016) 231−240.

[58] Y. Xu, Y. Yuan, A. Ma, X. Wu, Y. Liu, B. Zhang, Composition-tunable Pt-Co alloy nanoparticle networks: facile room-temperature synthesis and supportless electrocatalytic applications, ChemPhysChem 13 (2012) 2601−2609.

[59] L. Zhang, D. Lu, Y. Chen, Y. Tang, T. Lu, Facile synthesis of Pd−Co−P ternary alloy network nanostructures and their enhanced electrocatalytic activity towards hydrazine oxidation, J. Mater. Chem. A 2 (2014) 1252−1256.

[60] D.C. de Oliveiraa, W.O. Silvaa, M. Chatenet, F.H.B. Lima, NiO_x-Pt/C nanocomposites: highly active electrocatalysts for the electrochemical oxidation of hydrazine, Appl. Catal. B Environ. 201 (2017) 1−7.

[61] S. Jiang, Y. Ma, G. Jian, H. Tao, X. Wang, Y. Fan, et al., Facile construction of Pt−Co/CNx nanotube electrocatalysts and their application to the oxygen reduction reaction, Adv. Mater. 21 (2009) 4953−4956.

[62] Y. Uemura, Y. Inada, K.K. Bando, T. Sasaki, N. Kamiuchi, K. Eguchi, A. Yagishita, M. Nomura, M. Tada, Y. Iwasawa, Core-shell phase separation and structural transformation of pt_3sn alloy nanoparticles supported on γ-Al_2O_3 in the reduction and oxidation processes characterized by in situ time-resolved XAFS, J. Phys. Chem. C 115 (2011) 5823−5833.

https://doi.org/10.1016/j.heliyon.2019.e01380
2405-8440/© 2019 Published by Elsevier Ltd. This is an open access article under the CC BY-NC-ND license (http://creativecommons.org/licenses/by-nc-nd/4.0/).

[63] X. Wang, W. Lia, Z. Chen, M. Waje, Y. Ya, Durability investigation of carbon nanotube as catalyst support for proton exchange membrane fuel cell, J. Power Sources 158 (2006) 154−159.

[64] J.M. Campelo, D. Luna, R. Luque, J.M. Marinas, A.A. Romero, Sustainable preparation of supported metal nanoparticles and their applications in catalysis, ChemSusChem 2 (2009) 18−45.

[65] F. Rodriguez-Reinoso, The role of carbon materials in heterogeneous catalysis, Carbon 36 (1998) 159−175.

[66] K. Vignarooban, J. Lin, A. Arvay, S. Kolli, I. Kruusenberg, K. Tammeveski, L. MunukutlaA, M. Kannan, Nano-electrocatalyst materials for low temperature fuel cells: a review, Chin. J. Catal. 36 (2015) 458−472.

[67] P. Trogadas, T.F. Fuller, P. Strasser, Carbon as catalyst and support for electrochemical energy conversion, Carbon 75 (2014) 5−42.

[68] C. Subban, Q. Zhou, B. Leonard, C. Ranjan, H.M. Edvenson, F.J. DiSalvo, et al., Catalyst supports for polymer electrolyte fuel cells, Philos. Trans. R. Soc. A Math. Phys. Eng. Sci. 368 (2010) 3243−3253.

[69] J. Wu, X.Z. Yuan, J.J. Martin, H.J. Wang, J.J. Zhang, J. Shen, S.H. Wu, W. Merida, A review of PEM fuel cell durability: degradation mechanisms and mitigation strategies, J. Power Sources 184 (2008) 104−119.

[70] V. Kamavaram, V. Veedu, A.M. Kannan, Synthesis and characterization of platinum nanoparticles on in situ grown carbon nanotubes based carbon paper for proton exchange membrane fuel cell cathode, J. Power Sources 188 (2009) 51−56.

[71] M.L. Toebes, M. van der Lee, L.M. Tang, M.H.H. in't Veld, J.H. Bitter, A.J. van Dillen, K.P. de Jong, Preparation of carbon nanofiber supported platinum and ruthenium catalysts: comparison of ion adsorption and homogeneous deposition precipitation, J. Phys. Chem. B 108 (2004) 11611−11619.

[72] J. Arjomandi, S. Tadayyonfar, Electrochemical synthesis and in situ spectroelectrochemistry of conducting polymer nanocomposites. I. polyaniline/TiO_2, polyaniline/ZnO, and polyaniline/TiO_2+ZnO, Polym. Compos. 35 (2014) 351−363.

[73] M. Trueba, S.P. Trasatti, γ-Alumina as a support for catalysts: a review of fundamental aspects, Eur. J. Inorg. Chem. 2005 (2005) 3393−3403.

[74] J.R. Windmiller, A.J. Bandodkar, S. Parkhomovsky, J. Wang, Stamp transfer electrodes for electrochemical sensing on non-planar and oversized surfaces, Analyst 137 (2012) 1570−1575.

 https://doi.org/10.1016/j.heliyon.2019.e01380
2405-8440/© 2019 Published by Elsevier Ltd. This is an open access article under the CC BY-NC-ND license (http://creativecommons.org/licenses/by-nc-nd/4.0/).

[75] S. Dong, T. Kuwana, Activation of glassy carbon electrodes by dispersed metal oxide particles, J. Electrochem. Soc. 131 (1984) 813–819.

[76] B.R. Kozub, N.V. Rees, R.G. Compton, Electrochemical determination of nitrite at a bare glassy carbon electrode; why chemically modify electrodes? Sensor. Actuator. B Chem. 143 (2010) 539–546.

[77] S. Basu, A. Shegokar, D. Biswal, Synthesis and characterization of supported Sn/γ-Al_2O_3 and Sn/ZSM5 catalysts for CO_2 reduction in electrochemical cell, J. CO_2 Util. 18 (2017) 80–88.

[78] M.H. Parvin, J. Arjomandi, J.Y. Lee, γ-Al_2O_3 nanoparticle catalyst mediated polyaniline gold electrode biosensor for vitamin E, Catal. Commun. 110 (2018) 59–63.

[79] C. Ma, Y. Chang, W. Ye, W. Shang, C. Wang, Supercritical preparation of hexagonal γ -alumina nanosheets and its electrocatalytic properties, J. Colloid Interface Sci. 317 (2008) 148–154.

[80] N. Firdous, N.K. Janjua, I. Qazi, M.H.S. Wattoo, Optimal Co–Ir bimetallic catalysts supported on γ-Al_2O_3 for hydrogen generation from hydrous hydrazine, Int. J. Hydrogen Energy 41 (2016) 984–995.

[81] A. Islam, Y.H. Taufiq-Yap, C.-M. Chu, E.-S. Chan, P. Ravindra, Synthesis and characterization of millimetric gamma alumina spherical particles by oil drop granulation method, J. Porous Mater. 19 (2012) 807–817.

[82] F. Pinna, Supported metal catalysts preparation, Catal. Today 41 (1998) 129–137.

[83] J. Mathiyarasu, A. Remona, A. Mani, K. Phani, V. Yegnaraman, Exploration of electrodeposited platinum alloy catalysts for methanol electro-oxidation in 0.5 M H_2SO_4: Pt-Ni system, J. Solid State Electrochem. 8 (2004) 968–975.

[84] T.C. Deivaraj, W. Chen, J.Y. Lee, Preparation of PtNi nanoparticles for the electrocatalytic oxidation of methanol, J. Mater. Chem. 13 (2003) 2555–2560.

[85] B. Naik, V. Prasad, N. Ghosh, Development of a simple aqueous solution based chemical method for synthesis of mesoporous γ-alumina powders with disordered pore structure, J. Porous Mater. 17 (2010) 115–121.

[86] A. Khaleel, S. Al-Mansouri, Meso-macroporous γ-alumina by template-free sol–gel synthesis: the effect of the solvent and acid catalyst on the microstructure and textural properties, Colloid. Surf. A Physicochem. Eng. Asp. 369 (2010) 272–280.

https://doi.org/10.1016/j.heliyon.2019.e01380
2405-8440/© 2019 Published by Elsevier Ltd. This is an open access article under the CC BY-NC-ND license (http://creativecommons.org/licenses/by-nc-nd/4.0/).

[87] N.K. Janjua, N. Firdous, A.S. Bhatti, Z.S. Khan, Preparation and catalytic evaluation of Ir and Ru catalysts supported in γ-Al_2O_3 for hydrazine decomposition in a 1N microthruster, Appl. Catal. A Gen. 479 (2014) 9−16.

[88] A. Kogelbauer, J.G. Goodwin Jr., R. Oukaci, Ruthenium promotion of Co/Al_2O_3 Fischer−Tropsch catalysts, J. Catal. 160 (1996) 125−133.

[89] C.L. Bianchi, TPR and XPS investigations of Co/Al_2O_3 catalysts promoted with Ru, Ir and Pt, Catal. Lett. 76 (2001) 155−159.

[90] A.R. Belambe, R. Oukaci, J. Goodwin Jr., Effect of pretreatment on the activity of a Ru-promoted Co/Al_2O_3 Fischer−Tropsch catalyst, J. Catal. 166 (1997) 8−15.

[91] B. Sexton, A. Hughes, T. Turney, An XPS and TPR study of the reduction of promoted cobalt-kieselguhr Fischer-Tropsch catalysts, J. Catal. 97 (1986) 390−406.

[92] L. Backman, A. Rautiainen, M. Lindblad, A. Krause, The interaction of cobalt species with alumina on Co/Al_2O_3 catalysts prepared by atomic layer deposition, Appl. Catal. A Gen. 360 (2009) 183−191.

[93] M. El Doukkali, A. Iriondo, P. Arias, J. Requies, I. Gandarías, L. Jalowiecki-Duhamel, F. Dumeignil, A comparison of sol−gel and impregnated Pt or/and Ni based γ-alumina catalysts for bioglycerol aqueous phase reforming, Appl. Catal. B Environ. 125 (2012) 516−529.

[94] G. Batley, A. Ekstrom, D. Johnson, Studies of topochemical heterogeneous catalysis: 3. Catalysis of the reduction of metal oxides by hydrogen, J. Catal. 34 (1974) 368−375.

[95] D.J. Suh, C. Kwak, J.-H. Kim, S.M. Kwon, T.-J. Park, Removal of carbon monoxide from hydrogen-rich fuels by selective low-temperature oxidation over base metal added platinum catalysts, J. Power Sources 142 (2005) 70−74.

[96] G. Jacobs, T.K. Das, Y. Zhang, J. Li, G. Racoillet, B.H. Davis, Fischer−-Tropsch synthesis: support, loading, and promoter effects on the reducibility of cobalt catalysts, Appl. Catal. A Gen. 233 (2002) 263−281.

[97] T. Sakamoto, T. Masuda, K. Yoshimoto, H. Kishi, S. Yamaguchi, D. Matsumura, K. Tamura, A. Hori, Y. Horiuchi, A. Serov, NiO/Nb_2O_5/C hydrazine electrooxidation catalysts for anion exchange membrane fuel cells, J. Electrochem. Soc. 164 (2017) F229−F234.

https://doi.org/10.1016/j.heliyon.2019.e01380
2405-8440/© 2019 Published by Elsevier Ltd. This is an open access article under the CC BY-NC-ND license (http://creativecommons.org/licenses/by-nc-nd/4.0/).

[98] H.R. Zare, N. Nasirizadeh, Electrocatalytic characteristics of hydrazine and hydroxylamine oxidation at coumestan modified carbon paste electrode, Electroanalysis 18 (2006) 507–512.

[99] H.R. Zare, N. Nasirizadeh, S.-M. Golabi, M. Namazian, M. Mazloum-Ardakani, D. Nematollahi, Electrochemical evaluation of coumestan modified carbon paste electrode: study on its application as a NADH biosensor in presence of uric acid, Sensor. Actuator. B Chem. 114 (2006) 610–617.

[100] T. Rebis, S. Lijewski, J. Nowicka, L. Popenda, L. Sobotta, S. Jurga, J. Mielcarek, G. Milczarek, T. Goslinski, Electrochemical properties of metallated porphyrazines possessing isophthaloxybutylsulfanyl substituents: application in the electrocatalytic oxidation of hydrazine, Electrochim. Acta 168 (2015) 216–224.

https://doi.org/10.1016/j.heliyon.2019.e01380
2405-8440/© 2019 Published by Elsevier Ltd. This is an open access article under the CC BY-NC-ND license (http://creativecommons.org/licenses/by-nc-nd/4.0/).